International Journal of Nanomedicine

Dovepress
Taylor & Francis Group

Open Access Full Text Article

ORIGINAL RESEARCH

Amine-Functionalized $NiCoFe_2O_4$ Nanoparticle–Embedded Sodium Alginate/Polyvinyl Alcohol Hydrogel Beads as a ROS-Generating, pH-Responsive Drug Carrier

Ujwala Guntakanti[1], Sreekanth Reddy Obireddy[2], Chong Yu[2], Yong-Rui Su[3], Karuna Sree Merugu[4], Anitha Kowthalam[5], Wing-Fu Lai[6]

[1]Department of Chemistry, G. Pulla Reddy Engineering College, Kurnool, AP, 518 007, India; [2]Department of Urology, Zhejiang Provincial People's Hospital, Affiliated People's Hospital, Hangzhou Medical College, Hangzhou, Zhejiang, 310014, People's Republic of China; [3]The second Clinical Medical College, Zhejiang Chinese Medical University, Hangzhou, Zhejiang, 310014, People's Republic of China; [4]Department of Chemistry, GITAM School of Science, GITAM Deemed to Be University, Bengaluru, KA, 562163, India; [5]Department of Chemistry, Sri Krishnadevaraya University, Ananthapur, AP, 515003, India; [6]School of Food Science and Nutrition, University of Leeds, Leeds, LS2 9JT, UK

Correspondence: Wing-Fu Lai; Anitha Kowthalam, Email rori0610@graduate.hku.hk; anitbios@gmail.com

Introduction: Metal oxide nanoparticle–loaded hydrogel beads have recently emerged as a promising tool for controlled release applications. This study explores the synthesis and characterization of amine-functionalized nickel cobalt ferrite ($NiCoFe_2O_4$) nanoparticles (ANiCoFe NPs) embedded within sodium alginate/polyvinyl alcohol (SAPVA) hydrogel beads for the controlled release of 5-fluorouracil (5-FU).

Methods: ANiCoFe NPs were synthesized via chemical co-precipitation, and the NP-loaded hydrogel beads were prepared using ionotropic gelation. The hydrogel beads were characterized by various techniques including FTIR, XRD and TGA. In vitro release studies were performed at pH 7.4 and 2.0 at 37°C, and cytotoxicity was evaluated on MCF-7 and MCF-10 cells.

Results: Scanning electron microscopy revealed a highly porous hydrogel structure. Thermal and degradation analyses demonstrated that NP incorporation enhanced hydrogel stability. Release studies confirmed pH-responsive behaviour. Cytotoxicity assays showed that 5-FU/NP-loaded beads significantly reduced MCF-7 cell viability, whereas SAPVA and NP-loaded beads without drug exhibited negligible toxicity toward MCF-10 cells.

Discussion: The developed hydrogel beads are pH-responsive and provide controlled drug release, with their ROS-generating capability enhancing their potential for therapeutic applications.

Keywords: nickel cobalt ferrite nanoparticles, sodium alginate, polyvinyl alcohol, hydrogel beads, drug delivery, controlled release

Introduction

In recent years, nanotechnology has opened new opportunities in the biomedical field,[1–4] particularly with metal- and metal oxide-based nanoparticles (NPs), which have received significant interest due to their unique physicochemical properties. However, the application of nanomaterials in disease treatment faces limitations. While many nanomaterials demonstrate good biocompatibility in both in vitro and in vivo animal models, this consistency is often not observed in human clinical trials.[5–7] Moreover, the dissolution of metal oxide NPs can release metal ions, potentially destabilizing phagolysosomes and inducing inflammatory responses.[8] Therefore, comprehensive analyses of pharmacokinetics, pharmacodynamics, biodistribution, and long-term toxicity are essential for evaluating nanomaterials during treatment.

To address the toxicity of pristine NPs, polymer-based nanocomposites have been developed. These nanocomposites exhibit enhanced oral bioavailability, controlled release, and low toxicity with minimal side effects.[9,10] They are typically prepared by dispersing NPs throughout a polymeric matrix.[11,12] Nanocomposite hydrogels are particularly advantageous

Received: 26 May 2025
Accepted: 11 December 2025
Published: 30 December 2025

as drug carriers due to their improved properties relative to pure polymer hydrogels. NP incorporation can reduce burst release, enhance drug stability, and enable controlled and sustained drug release.[13–16] For example, ibuprofen-loaded chitosan/ZnO nanocomposites exhibited slower release rates compared with chitosan nanocomposites without ZnO.[16] Similarly, incorporating ZnO NPs into polymer matrices enhances drug encapsulation efficiency in nanocomposites,[17] and zinc oxide NPs have been used to create alginate composite hydrogel beads for controlled release of curcumin.[18] Furthermore, amine-functionalized magnetic NP-loaded sodium alginate and xanthan gum microbeads have been employed for controlled levofloxacin release and antibacterial applications.[19]

Metal oxide NPs are attractive as drug carriers due to their large surface area, magnetic properties, and potential for precise targeting and controlled release.[20] Diverse metal oxide NPs have also demonstrated anticancer and antibacterial properties.[21,22] For instance, carbon quantum dots and copper oxide-functionalized Fe_2O_3 magnetic NP-loaded galactomannan and sodium alginate bio-nanocomposite hydrogels have been used to deliver doxorubicin, exhibiting both anticancer and antibacterial activity.[23] Similarly, folate-conjugated DOX/CS/rGO/NiO nanocomposites have demonstrated anticancer activity against MCF-7 and A549 cells, along with antimicrobial effects.[24] Among metal oxide NPs, iron oxide NPs have received attention for biomedical applications due to their non-toxic behaviour in biological systems,[25] and their reported anticancer and antimicrobial effects.[26] Other NPs, such as nickel ferrite NPs, have shown anticancer effects against MCF-7 cells, suggesting their potential in cancer treatment.[27] Cobalt ferrite magnetic NPs have also exhibited antitumor effects via magnetic hyperthermia.[28,29]

In this study, we prepared amine-functionalized nickel cobalt ferrite (ANiCoFe) NPs loaded into sodium alginate (SA)/polyvinyl alcohol (PVA) hydrogel beads and investigated their in vitro drug release and cytotoxicity. SA and PVA were selected for their biocompatibility, biodegradability, and film-forming ability.[30,31] Incorporating metal oxide NPs into hydrogel beads also improves mechanical strength, crosslinking capacity, and thermal stability.[32] 5-Fluorouracil (5-FU) was used as a model drug because it inhibits cancer cell proliferation by disrupting DNA synthesis.[33] Upon loading with 5-FU, the hydrogel beads exhibited pH-sensitive drug release and in vitro cytotoxicity against MCF-7 cells, demonstrating their potential as effective carriers for controlled drug delivery.

Materials and Methods

Materials

Polyvinyl alcohol and $CaCl_2$ were purchased from Merck (Mumbai, India). Sodium alginate, 5-fluorouracil, nickel(II) nitrate hexahydrate, cobalt(II) nitrate hexahydrate, iron(III) nitrate nonahydrate, ethylenediamine, ethylene glycol, sodium hydroxide, and ethanol were obtained from SD Fine-Chem Limited (Mumbai, India). Human milk lysozyme was purchased from MedChemExpress.

Synthesis of ANiCoFe NPs

ANiCoFe NPs were synthesized by dissolving stoichiometric amounts of $Ni(NO_3)_2 \cdot 6H_2O$ (0.559 g), $Co(NO_3)_2 \cdot 6H_2O$ (0.560 g), and $Fe(NO_3)_3 \cdot 9H_2O$ (0.775 g) in 20 mL of water, followed by stirring for 3 hours. The pH of the solution was adjusted to 12 using 2 M sodium hydroxide. Subsequently, 200 µL of ethylenediamine and 500 µL of ethylene glycol were added, and the mixture was stirred for 1 hour. The temperature was then raised to 80°C, and the solution was stirred for an additional hour. After cooling, the precipitate was collected by centrifugation at 10,000 rpm for 10 minutes and washed with a water–ethanol mixture to remove residual ethylenediamine and ethylene glycol. The final product was dried at 80°C and annealed at 550°C for 6 hours to obtain ANiCoFe NPs. Nickel cobalt ferrite (NiCoFe) NPs were prepared using the same procedure, omitting ethylenediamine.

Synthesis of Hydrogel Beads

Hydrogel beads were synthesized using a gelation technique.[34] 300 mg each of SA and PVA were separately dissolved in 10 mL of distilled water under constant stirring for 6 hours. The SA and PVA solutions were then combined and stirred until a homogeneous blend was obtained. To this mixture, varying amounts of 5-FU and ANiCoFe NPs, as listed in Table 1, were added, sonicated for 15 minutes, and stirred continuously for 3 hours. The resulting solution was added dropwise into calcium chloride solution using a syringe, inducing gelation via calcium ions and forming hydrogel beads.

Table 1 Formulation Compositions of Different Hydrogel Beads

	SA (mg)	PVA (mg)	NPs (mg)	5-FU (mg)
SAPVA-5-FU	300	300	000	100
SAPVA-ANPs	300	300	100	000
SAPVA-ANPs-5-FU	300	300	100	100
SAPVA	300	300	000	000

The hydrogel beads were collected, washed with water to remove excess calcium chloride and unbound 5-FU, and dried overnight at 40°C.

Structural Characterization

FTIR spectra of the hydrogel beads, NPs, and 5-FU were recorded using a FTIR spectrometer (Bomem MB-3000, Canada) in the range of 400–4000 cm^{-1}. X-ray diffraction (XRD) patterns of 5-FU, NPs, and hydrogel beads were obtained using a Rigaku MiniFlex600 diffractometer (Japan) at a scanning rate of 10°/min. To examine surface morphology and topography, the hydrogel beads were analyzed by scanning electron microscopy (SEM, JEOL IT500A, Japan). The particle size of the NPs was determined using transmission electron microscopy (TEM, JEOL JEM 2100, Japan).

Determination of Encapsulation Efficiency and Release Kinetics

The encapsulation efficiency (EE) of hydrogel beads containing 5-FU was determined as previously reported.[35] Drug release studies were performed using dissolution analysis. Briefly, 30 mg of hydrogel beads were placed in a dialysis bag and immersed in 150 mL of phosphate-buffered saline (PBS) at pH 2.0 and 7.4 and 37°C, with stirring at 50 rpm. At predetermined time intervals, 3 mL of the release medium was withdrawn and analyzed at 260 nm using a UV-Vis spectrophotometer. The amount of 5-FU released was quantified by comparison with a calibration curve. Withdrawn volumes were replaced with equal volumes of fresh PBS to maintain sink conditions. To investigate the release kinetics and mechanism, the drug release profiles were fitted to various models, including zero-order, first-order, Higuchi, and Korsmeyer–Peppas models.[36]

Degradation Studies

Precisely weighed 10 mg of hydrogel beads were immersed in 5 mL of PBS (pH 1.2 and 7.4), with or without lysozyme and incubated at 37°C. At predetermined time intervals, the hydrogel beads were retrieved, air-dried, and the percentage degradation was calculated based on the weight difference before and after incubation.

Cytotoxicity Studies

The cytotoxicity of hydrogel beads against MCF-7 (obtained from NCCS, Pune, India) and MCF-10 cells (obtained from ATCC, USA) was evaluated using the MTT assay. Briefly, 20,000 cells per well were seeded in a 96-well plate and incubated at 37°C in 5% CO_2 for 24 h. Cells were then treated with the test samples at the desired concentrations and incubated for 48 h. Following treatment, 500 µg/mL of MTT reagent was added to each well, and the plate was incubated for 3 h at 37°C under 5% CO_2. The medium was subsequently replaced with 100 µL of DMSO per well, and the plate was agitated on a gyratory shaker. Absorbance was measured at 570 nm. In addition to the MTT assay, the ROS-generating capacity of treated cells was assessed according to previously established protocols.[35]

Statistical Analysis

All data are presented as mean ± standard deviation calculated from triplicate measurements. Graphs and descriptive statistics were prepared using Origin.

Results and Discussion

Structural Characterization

The FTIR spectra of 5-FU, SAPVA, SAPVA-5-FU, NiCoFe NPs, ANiCoFe NPs, SAPVA-ANPs, and SAPVA-ANPs-5-FU are shown in Figure 1. The spectrum of 5-FU exhibited peaks at 1250, 1679, 2931, 3100, and 3220 cm^{-1}, corresponding to C–F, C=O, $–CH_2$, =C–H, and N–H stretching frequencies, respectively.[37] The NiCoFe NPs displayed characteristic peaks at 556 and 462 cm^{-1}, associated with the stretching vibrations of tetrahedral and octahedral sites in the spinel structure.[38] The amine-functionalized NiCoFe NPs showed peaks similar to those of the unmodified NiCoFe NPs; however, the appearance of new bands at 1066 cm^{-1} and 3407 cm^{-1}, attributed to C–N and N–H stretching frequencies, confirmed the presence of ethylenediamine molecules on the NP surface. SAPVA exhibited characteristic peaks at 1122, 1596, and 3425 cm^{-1}, corresponding to C–O, C=O, and O–H stretching vibrations, respectively. Upon loading with 5-FU, a new peak appeared at 803 cm^{-1}, along with a broadening of the peak at 1137 cm^{-1}, likely due to the presence of 5-FU within the SAPVA matrix, indicating successful encapsulation.[39] A blue shift of the C=O band to 1601 cm^{-1} was also observed in SAPVA-5-FU hydrogel beads, attributed to intermolecular interactions between 5-FU and the polymer matrix. The spectrum of SAPVA-ANPs-5-FU displayed a pattern similar to SAPVA-5-FU, along with a new peak at 553 cm^{-1}, confirming the successful incorporation of ANiCoFe NPs into the hydrogel beads. Likewise, the spectra of SAPVA-ANPs resembled that of SAPVA, with a distinct new band at 549 cm^{-1}, further validating the presence of NPs within the hydrogel beads.

The crystalline structures of 5-FU, NiCoFeO NPs, SAPVA, SAPVA-5-FU, SAPVA-ANPs-5-FU, and SAPVA-ANPs were further confirmed by XRD, and the corresponding diffraction patterns are shown in Figure 2. The NiCoFeO NPs displayed characteristic diffraction peaks at 2θ values of 18.2°, 29.96°, 35.4°, 37.06°, 42.96°, 53.3°, and 56.81°, corresponding to the (111), (220), (311), (222), (400), (422), (511), (440), and (533) planes. These reflections matched JCPDS cards 22–1086 and 44–1485, confirming the formation of a spinel-structured NiCoFeO NPs.[38] Pure 5-FU exhibited a distinct crystalline peak at 28.7°, which disappeared in both SAPVA-5-FU and SAPVA-ANPs-5-FU. This loss of crystallinity suggests that 5-FU was molecularly dispersed or amorphized within the polymer matrix.[40] Furthermore, the diffraction pattern of SAPVA-ANPs retained the characteristic peaks of NiCoFeO NPs, indicating that the NPs remained crystalline after incorporation and were successfully embedded within the SAPVA hydrogel beads.[41]

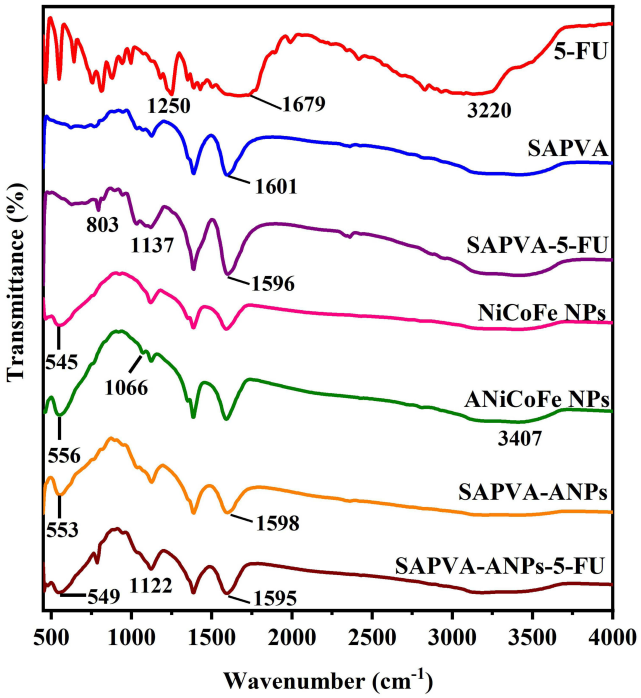

Figure 1 FTIR spectra of 5-FU, SAPVA, SAPVA-5-FU, NiCoFe NPs, ANiCoFe NPs, SAPVA-ANPs and SAPVA-ANPs-5-FU.

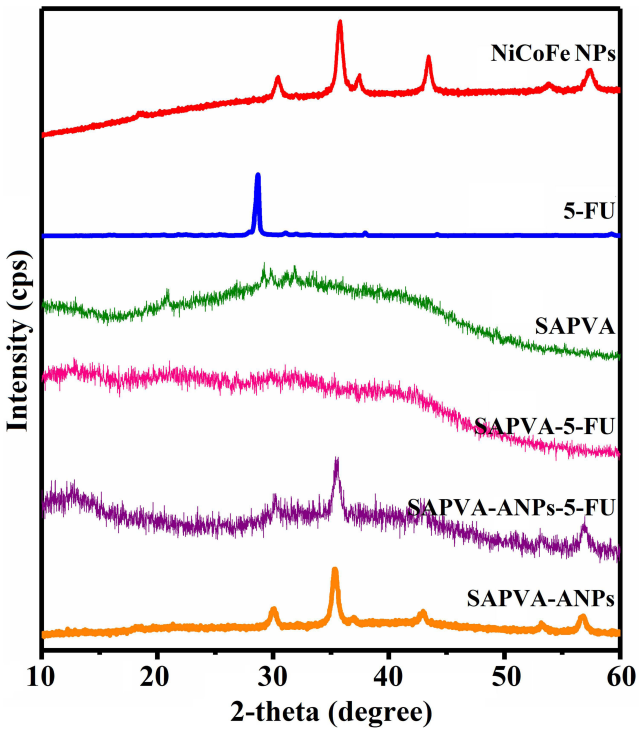

Figure 2 XRD patterns of NiCoFe NPs, 5-FU, SAPVA, SAPVA-5-FU, SAPVA-ANPs-5-FU, and SAPVA-ANPs.

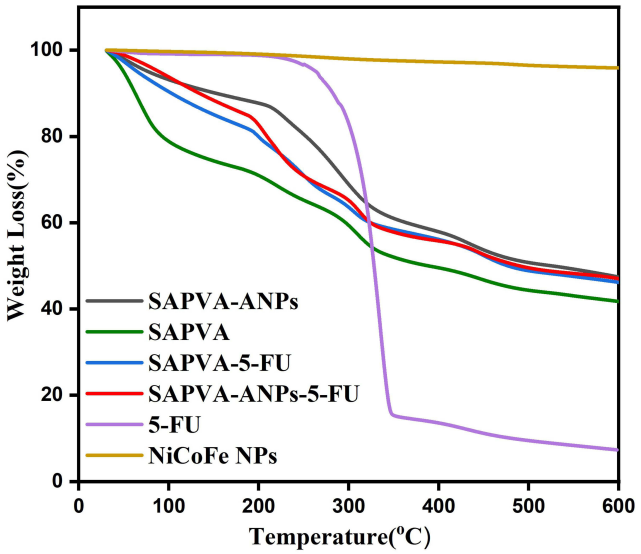

Figure 3 TGA graphs of SAPVA-ANPs, SAPVA, SAPVA-5-FU, SAPVA-ANPs-5-FU, 5-FU, and NiCoFe NPs.

Thermogravimetric analysis (TGA) was performed to assess the thermal stability of the prepared compounds (Figure 3). The thermogram of 5-FU exhibited stable behavior up to 280°C, followed by a significant weight loss attributed to the decomposition of 5-FU.[42] SAPVA displayed three distinct weight-loss stages: the first, between 27–100°C, showed a weight loss of ~21%, corresponding to the evaporation of moisture. The second and third stages, occurring between 100–330°C and 330–600°C with weight losses of ~20% and ~14%, respectively, were associated with decarboxylation of COOH groups and decomposition of the remaining polymeric material. The thermograms of SAPVA-5-FU, SAPVA-ANPs-5-FU, and SAPVA-ANPs exhibited similar thermal behavior, with slight variations in weight loss

https://doi.org/10.2147/IJN.S542903

percentages due to the incorporation of 5-FU and NPs into the polymer matrix. SAPVA showed a phase transition peak at ~190 °C, whereas the peak for SAPVA-ANPs shifted to 212 °C, indicating that the inclusion of NPs enhanced the thermal stability of the hydrogel beads. Moreover, the total weight loss of SAPVA at 600 °C (~59%) was higher than that of SAPVA-ANPs, further confirming that NP incorporation improves thermal stability. A similar observation was reported previously,[43] in which the inclusion of Zn^{2+} or graphene oxide into the alginate matrix was demonstrated to enhance thermal stability compared with neat sodium alginate.

SEM and TEM Analysis

Surface morphology plays a crucial role in drug delivery applications. The morphology of the prepared compounds was examined using SEM and TEM, and the results are presented in Figure 4. SAPVA exhibited a smooth, non-porous surface, indicating good compatibility between sodium alginate and PVA. Upon loading 5-FU into the polymer matrix, small pores appeared on the surface of SAPVA-5-FU. The incorporation of NPs into the polymer matrix resulted in SAPVA-ANPs-5-FU exhibiting a rougher surface with higher porosity, suggesting that the NPs influenced the hydrogel morphology. The average size of the hydrogel beads ranged from 600 to 900 μm. TEM analysis provided insights into the NP size, as shown in Figure 4. The NPs were observed to be in the range of 10–30 nm. Overall, these morphological studies demonstrate that the porous surface of the hydrogel beads is crucial for facilitating drug release.

Degradation Studies

Degradation of hydrogel beads was evaluated at different pH levels (7.4 and 2.0), and the results are presented in Figure 5. The hydrogel beads exhibited faster degradation at pH 7.4 than at pH 2.0. This behavior is attributed to the looser hydrogel network at pH 7.4. Additionally, sodium ions in the solvent can replace calcium ions in the polymer matrix, weakening the network and accelerating degradation.[44] In contrast, under acidic conditions (pH 2.0), the hydrogel beads demonstrated greater stability due to the limited solubility of the polymer matrix. The effect of lysozyme on the degradation rate was also examined at both pH levels. Incorporation of lysozyme in PBS slightly increased degradation compared to PBS alone. Approximately 50% degradation was observed in SAPVA hydrogel beads by the 14th day, consistent with findings by Bahadoran and coworkers,[45] who reported that a 50:50 SA/PVA blend hydrogel exhibited ~50% degradation after four weeks. Furthermore, the impact of NPs on degradation was investigated. SAPVA-ANPs exhibited a slower degradation rate compared to SAPVA, likely due to interactions between NPs and polymer chains via hydrogen bonding and electrostatic interactions, which strengthen the network and reduce degradation.

Drug Encapsulation and Release

The EE of 5-FU in SAPVA-5-FU and SAPVA-ANPs-5-FU was 71.6% and 74.8%, respectively. This increase in EE is attributed to the influence of NPs on the hydrogel bead surface. The incorporation of NPs enhances the porosity of the polymer network, facilitating greater encapsulation of 5-FU. Additionally, NPs interact with 5-FU molecules through hydrogen bonding and electrostatic interactions, further improving EE. This observation aligns with the findings of Gholamali and Yadollahi,[17] who reported higher EE in NP-loaded hydrogels. Figure 6A presents the results of in vitro release studies conducted at 37°C under different pH conditions (pH 2.0 and 7.4). These pH values were chosen to simulate physiological conditions: upon oral administration, the carriers first encounter the acidic environment of the stomach (pH ~2.0) and subsequently the intestine (pH ~7.0), while blood pH is approximately 7.4. The pKa of sodium alginate lies between 3.4 and 4.4; therefore, at pH 7.4, the carboxyl groups ionize into $–COO^-$ ions, increasing electrostatic repulsion within the hydrogel network. This loosens the matrix, facilitating the release of drug molecules. The impact of NPs on drug release was also investigated. SAPVA-ANPs-5-FU exhibited a slightly lower release rate compared with SAPVA-5-FU, due to hydrogen bonding and electrostatic interactions between NPs, the polymer network, and 5-FU. These interactions rigidify the network, slowing drug diffusion.[46]

To evaluate drug release kinetics and mechanism, the in vitro release data were fitted to several mathematical models, and the results are summarized in Table 2. The correlation coefficient (r^2) values indicated that the release profiles were consistent with both first-order and Higuchi models.[47] The drug release mechanism involves two steps: initial uptake of the release medium into the hydrogel beads, followed by diffusion of 5-FU into the surrounding environment. The release

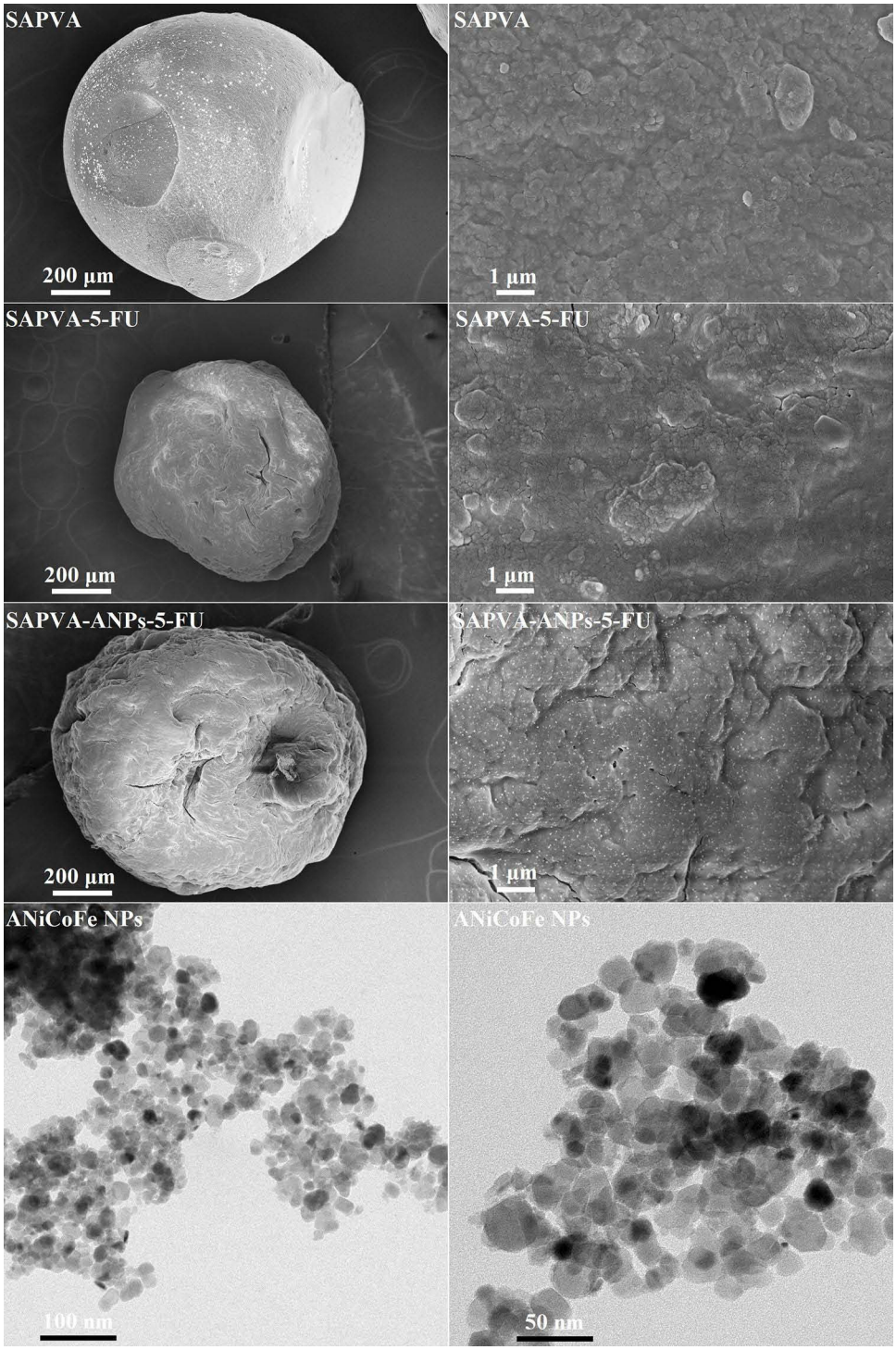

Figure 4 SEM images of SAPVA, SAPVA–5-FU, and SAPVA–ANPs–5-FU, and TEM images of ANiCoFe NPs.

rate correlated directly with the concentration of 5-FU. Notably, the kinetic constants (k) for the first-order and Higuchi models were lower for SAPVA-ANPs-5-FU than for SAPVA-5-FU, reflecting the slower release due to NP–drug interactions, as discussed above. Additionally, 60% of the release data were fitted to the Korsmeyer-Peppas model to investigate the release mechanism. The resulting release exponent (n) values ranged from 0.413 to 0.686, indicating non-Fickian diffusion. In SAPVA hydrogel beads, crosslinking between SA and PVA entrapped carboxylate groups of SA

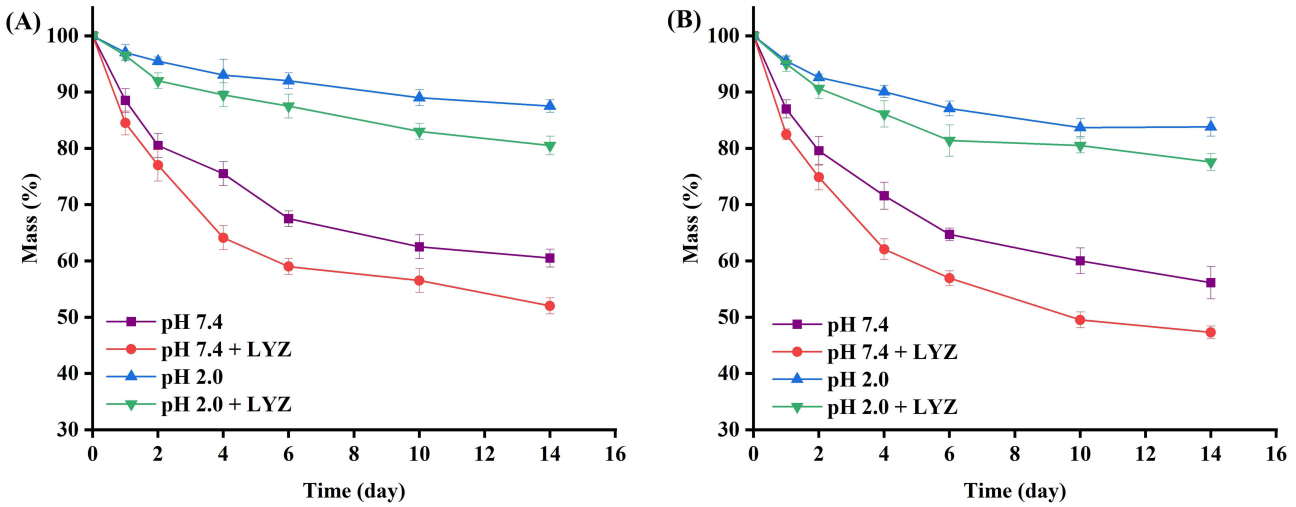

Figure 5 Degradation profiles of (**A**) SAPVA-ANPs and (**B**) SAPVA at 37°C.

within the polymeric network, reducing ionization and enhancing controlled diffusion of drug molecules, which contributed to the observed release pattern.[48]

Cytotoxicity and ROS-Generating Capacity

To assess the cytotoxicity of SAPVA and pristine ANiCoFe NPs, MTT assays were performed using MCF-10 cells, and the results are shown in Figure 6B. SAPVA showed more than 95% cell viability, while ANiCoFe NPs recorded 79% viability. These results indicate that the SAPVA matrix has good biocompatibility, while ANiCoFe NPs may exhibit a mild cytotoxic effect.[49] The cytotoxicity of 5-FU, SAPVA-5-FU, SAPVA-ANPs-5-FU, and SAPVA-ANPs was further evaluated in MCF-7 cells (Figure 6C). SAPVA-5-FU and SAPVA-ANPs-5-FU formulations significantly reduced cell viability, with 39.2% and 12.4% of cells remaining viable, respectively. Compared with free 5-FU, the slightly higher viability observed for SAPVA-5-FU and SAPVA-ANPs-5-FU reflects the sustained release of 5-FU from the hydrogel beads, which is advantageous for optimizing therapeutic outcomes while minimizing adverse effects. These results highlight the potential of SAPVA-5-FU and SAPVA-ANPs-5-FU as effective cancer treatment strategies. Moreover, SAPVA-ANPs demonstrated cytotoxic effects on MCF-7 cells, attributed to the generation of ROS. Similar observations have been reported in earlier studies on NP-based carriers.[21,50,51] ROS assays (Figure 6D) revealed fluorescence intensity in cells treated with NP-loaded hydrogel beads, indicating enhanced intracellular ROS levels induced by the NPs.[52]

Conclusion

ANiCoFe NPs were synthesized in this study and incorporated into the SA/PVA matrix to fabricate hydrogel beads via ionotropic gelation. FTIR and XRD analyses confirmed the successful formation of NPs and the molecular dispersion of 5-FU within the polymeric matrix. The incorporation of ANiCoFe NPs enhanced EE, thermal stability, and degradation behavior of the hydrogel beads. SEM analysis revealed that NPs increased the porosity and surface roughness of the hydrogel beads, while TEM confirmed NP sizes ranging from 10 to 30 nm. In vitro release studies demonstrated that the hydrogel beads were pH-responsive, with greater drug release at pH 7.4. The presence of NPs slightly modulated the release rate of 5-FU, indicating controlled release behavior. Cytotoxicity studies showed that SAPVA-5-FU and SAPVA-ANPs-5-FU effectively inhibited MCF-7 cancer cell viability, whereas SAPVA and ANiCoFe NPs exhibited minimal toxicity toward MCF-10 normal cells. This study has some limitations. The hydrogel beads exhibited size heterogeneity, which could be addressed in future studies by adopting advanced fabrication techniques to produce beads of uniform size. The EE was moderate and may be improved through optimization of the drug-loading process. Additionally, drug delivery efficacy was evaluated only in vitro, and preclinical studies are required to assess pharmacokinetics and therapeutic performance in vivo. Despite these limitations, the hydrogel beads

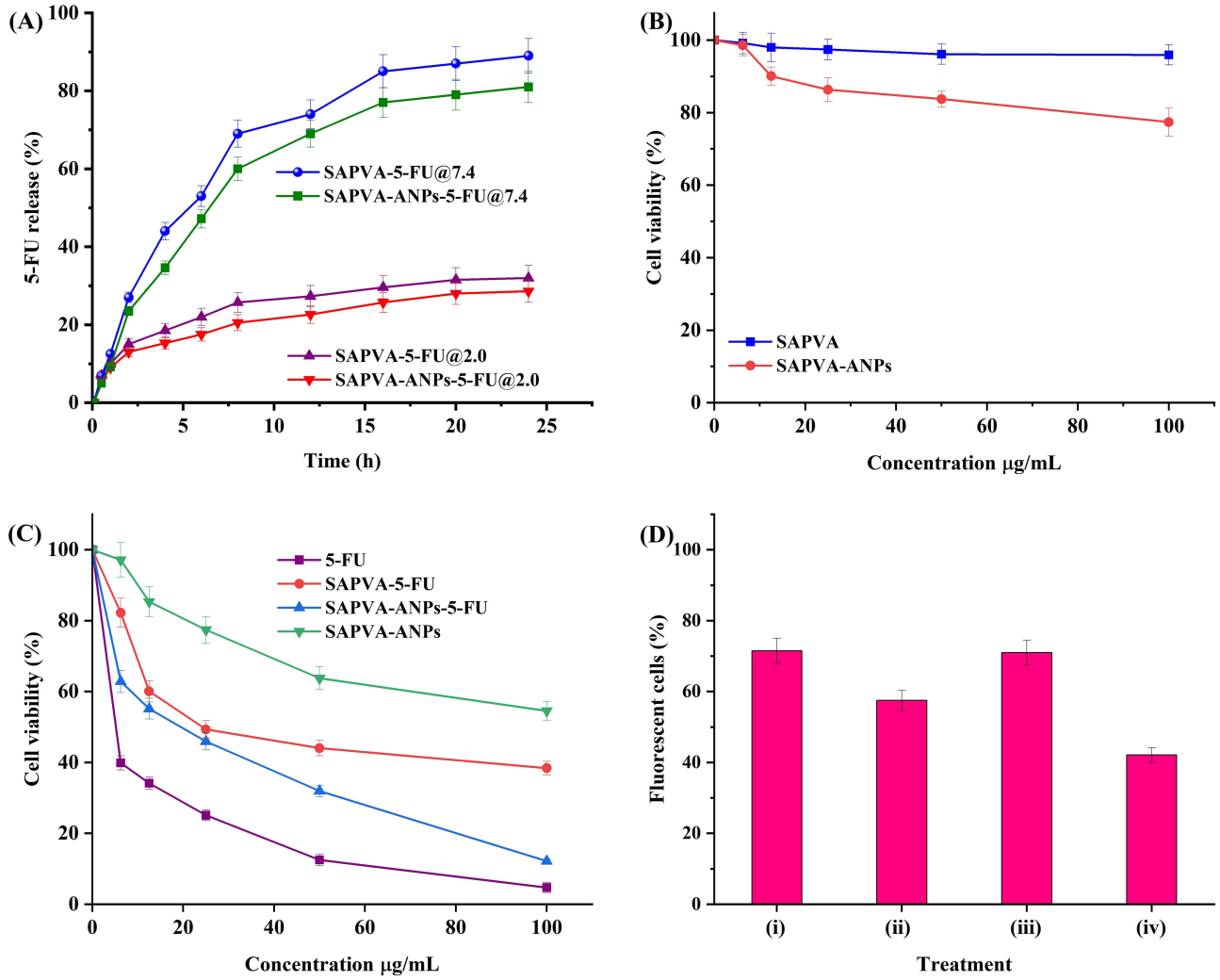

Figure 6 (**A**) In vitro release profiles of SAPVA-5-FU and SAPVA-ANPs-5-FU in PBS at pH 2.0 and 7.4 at 37°C. (**B**) Cell viability of MCF-10 cells treated with SAPVA and SAPVA-ANPs. (**C**) Cell viability of MCF-7 cells treated with 5-FU, SAPVA-5-FU, SAPVA-ANPs-5-FU, and SAPVA-ANPs. (**D**) ROS activity in MCF-7 cells after treatment under the following conditions: (i) treatment with 5-FU, (ii) treatment with SAPVA-5-FU, (iii) treatment with SAPVA-ANPs-5-FU, and (iv) treatment with SAPVA-ANPs.

demonstrated favorable properties, including pH-responsive drug release, ROS generation capability, and in vitro biocompatibility. These findings suggest that ANiCoFe NP-loaded hydrogel beads are promising candidates for controlled drug delivery applications and may be further developed as therapeutic carrier systems.

Table 2 Kinetic Parameters for 5-FU Release from All Hydrogel Beads in PBS at pH 2.0 and 7.4 at 37°C

	pH	Zero Order		First Order		Higuchi		Korsmeyer-Peppas	
		K_0	r^2	K_1	r^2	K_H	r^2	n	r^2
SAPVA-5-FU	7.4	4.836	0.6817	0.128	0.9865	20.197	0.9597	0.624	0.9739
	2.0	1.773	0.3130	0.023	0.4725	7.590	0.9078	0.433	0.9696
SAPVA-NPs-5-FU	7.4	4.371	0.7357	0.097	0.9775	18.142	0.9608	0.686	0.9834
	2.0	1.534	0.4287	0.019	0.5460	6.513	0.9421	0.413	0.9655

https://doi.org/10.2147/IJN.S542903

Disclosure

Dr. Wing-Fu Lai serves on the editorial board of this journal; however, he had no role in the editorial handling or in the peer-review process of this paper. The authors declare no other conflicts of interest.

References

1. Lai WF. Design and applications of polymersomes for oral drug administration. *ACS Appl Mater Interfaces*. 2025;17(21):30423–30435. doi:10.1021/acsami.5c04658
2. Obireddy SR, Liu K, Yu C, Zhang D, Wu GQ, Lai WF. Properties and use of chitosan/clay nanocomposites for drug delivery: a review. *Int J Biol Macromol*. 2025;318(Pt 2):144700. doi:10.1016/j.ijbiomac.2025.144700
3. Tripathi A, Pandey VK, Rustagi S, Lai WF, Samrot AV. Alginate-based NPs for targeted ovarian cancer therapy: navigating current progress and biomedical applications. *Int J Biol Macromol*. 2025;319(Pt 3):145365. doi:10.1016/j.ijbiomac.2025.145365
4. Lai W-F, Wong W-T, Rogach AL. Molecular design of layer-by-layer functionalized liposomes for oral drug delivery. *ACS Appl Mater Interfaces*. 2020;12(39):43341–43351. doi:10.1021/acsami.0c13504
5. Egbuna C, Parmar VK, Jeevanandam J, et al. Toxicity of nanoparticles in biomedical application: nanotoxicology. *J Toxicol*. 2021;2021(1):9954443. doi:10.1155/2021/9954443
6. Krishna R, Nagar V, Kaur A, et al. Toxicological effects of metal nanoparticles employed in biomedicine: biocompatibility, clinical trials, and future perspective. *Macromol Symp*. 2024;413(1):2300057. doi:10.1002/masy.202300057
7. Kilic A, Soylemez R. Various in vitro and in vivo current biomedical applications of metal oxide nanoparticles (MO NPs) from synthesis to spectroscopic studies: a brief review. *Biochem Biophys Res Commun*. 2025;786:152747. doi:10.1016/j.bbrc.2025.152747
8. Murthy S, Effiong P, Fei CC. Metal oxide nanoparticles in biomedical applications. In: Al-Douri Y, editor. *Metal Oxide Powder Technologies*. Elsevier; 2020:233–251.
9. Gupta I, Gandhi S, Sapra S. Metal/metal oxide nanoparticles reinforced biocomposites for drug delivery. In: Sharma N, Butola BS, editors. *Fiber and Textile Engineering in Drug Delivery Systems*. Woodhead Publishing; 2023:461–485.
10. Bamisaye A, Adekola MA, Abati SM, et al. Recent advances in metal/metal-oxide nanoparticle-polymer nanohybrid for biomedical applications. *Mater Today Chem*. 2025;49:103086. doi:10.1016/j.mtchem.2025.103086
11. Anwer AH, Ahtesham A, Shoeb M, et al. State-of-the-art advances in nanocomposite and bio-nanocomposite polymeric materials: a comprehensive review. *Adv Colloid Interface Sci*. 2023;318:102955. doi:10.1016/j.cis.2023.102955
12. Wawrzyńczak A, Chudzińska J, Feliczak-Guzik A. Metal and metal oxides nanoparticles as nanofillers for biodegradable polymers. *ChemPhysChem*. 2024;25(10):e202300823. doi:10.1002/cphc.202300823
13. Venkata Ramana E, Ujwala G, Shahinshavali S, Abdul Mathin S, Sreekanth Reddy O, Naseem. Development and evaluation of pH-responsive microbeads incorporated with nickel zinc ferrite nanoparticles for controlled release of doxorubicin. *ChemistrySelect*. 2024;9(41):e202402227. doi:10.1002/slct.202402227
14. Rathnam SR, Reddy OS, Gaikwad RS, Patwari SB. Development and characterization of copper nanoparticle-embedded pH-responsive polymeric microbeads for drug delivery and antibacterial applications. *ChemistrySelect*. 2023;8(32):e202301854. doi:10.1002/slct.202301854
15. Obireddy SR, Lai W-F. ROS-generating amine-functionalized magnetic nanoparticles coupled with carboxymethyl chitosan for pH-responsive release of doxorubicin. *Int J Nanomed*. 2022;17:589–601. doi:10.2147/IJN.S338897
16. Yadollahi M, Farhoudian S, Barkhordari S, Gholamali I, Farhadnejad H, Motasadizadeh H. Facile synthesis of chitosan/ZnO bio-nanocomposite hydrogel beads as drug delivery systems. *Int J Biol Macromol*. 2016;82:273–278. doi:10.1016/j.ijbiomac.2015.09.064
17. Gholamali I, Yadollahi M. Doxorubicin-loaded carboxymethyl cellulose/Starch/ZnO nanocomposite hydrogel beads as an anticancer drug carrier agent. *Int J Biol Macromol*. 2020;160:724–735. doi:10.1016/j.ijbiomac.2020.05.232
18. Zhang X, Xiao Y, Guo S, et al. pH-sensitive zinc oxide nanoparticle-controlled sodium alginate/silica hydrogel beads: for controlled curcumin release. *J Mol Struct*. 2025;1324:140967. doi:10.1016/j.molstruc.2024.140967
19. Rathnam SR, Reddy OS, Aravind S, Lai W-F, Patwari SB. Development of pH-sensitive microbeads incorporated with amine-functionalized magnetic nanoparticles for enhanced antibacterial activity. *ChemistrySelect*. 2024;9(37):e202400340. doi:10.1002/slct.202400340
20. Obireddy SR, Bellala S, Chintha M, Sake A, Subbarao SMC, Lai W-F. Synthesis and properties of alginate-based nanoparticles incorporated with different inorganic nanoparticulate modifiers for enhanced encapsulation and controlled release of favipiravir. *Arab J Chem*. 2023;16(7):104751. doi:10.1016/j.arabjc.2023.104751
21. Ramana EV, Naseem. Development and characterization of copper nanoparticles embedded polymeric microbeads for drug delivery and antibacterial applications. *Russ J Appl Chem*. 2022;95(9):1459–1466. doi:10.1134/S1070427222090221
22. Ma M, Pan Z, Zhu Z, et al. Enhanced cancer therapy using modified magnetic α-Fe_2O_3/Fe_3O_4 nanorods: dual role in curcumin delivery and ferroptosis induction. *Colloids Surf B Biointerfaces*. 2025;252:114689. doi:10.1016/j.colsurfb.2025.114689
23. Tahmasebi S, Mohammadi R. Green synthesis of pH-sensitive magnetic bio-nanocomposite hydrogel based on galactomannan and sodium alginate for targeted colorectal cancer drug delivery. *J Sci Adv Mater Devices*. 2025;10(2):100892. doi:10.1016/j.jsamd.2025.100892
24. Obireddy SR, Ayyakannu A, Kasi G, Sridharan B, Lai W-F, Viswanathan K. Folate-functionalized CS/rGO/NiO nanocomposites as a multifunctional drug carrier with anti-microbial, target-specific, and stimuli-responsive capacities. *Int J Nanomed*. 2025;20:1965–1981. doi:10.2147/IJN.S489418
25. Ganapathe LS, Mohamed MA, Mohamad yunus R, Berhanuddin DD. Magnetite (Fe_3O_4) nanoparticles in biomedical application: from synthesis to surface functionalisation. *Magnetochemistry*. 2020;6(4):68. doi:10.3390/magnetochemistry6040068
26. Hernández-Hernández AA, Aguirre-álvarez G, Cariño-Cortés R, Mendoza-Huizar LH, Jiménez-Alvarado R. Iron oxide nanoparticles: synthesis, functionalization, and applications in diagnosis and treatment of cancer. *Chem Pap*. 2020;74(11):3809–3824. doi:10.1007/s11696-020-01229-8
27. Sarala E, Vinuth M, Naik MM, Reddy YVR. Green synthesis of nickel ferrite nanoparticles using Terminalia catappa: structural, magnetic and anticancer studies against MCF-7 cell lines. *J Hazard Mater Adv*. 2022;8:100150.
28. Garanina AS, Nikitin AA, Abakumova TO, et al. Cobalt ferrite nanoparticles for tumor therapy: effective heating versus possible toxicity. *Nanomaterials*. 2021;12(1):38. doi:10.3390/nano12010038

29. Nagy Ľ, Zeleňáková A, Szűcsová J, Mielnik N, Hrubovcak P. Characterization of cobalt ferrite magnetic nanoparticles for magnetic hyperthermia application. *AIP Conf Proc*. 2023;2778(1):040020.
30. Gaaz TS, Sulong AB, Akhtar MN, Kadhum AA, Mohamad AB, Al-Amiery AA. Properties and applications of polyvinyl alcohol, halloysite nanotubes and their nanocomposites. *Molecules*. 2015;20(12):22833–22847. doi:10.3390/molecules201219884
31. Eswaramma S, Rao KSVK. Synthesis of dual responsive carbohydrate polymer based IPN microbeads for controlled release of anti-HIV drug. *Carbohydr Polym*. 2017;156:125–134. doi:10.1016/j.carbpol.2016.09.023
32. Saadatidizaji Z, Sohrabi N, Mohammadi R, Amini-Fazl MS. Tetracycline hydrochloride loaded-alginate based nanoparticle-hydrogel beads for potential wound healing applications: in vitro drug delivery, release kinetics, and antibacterial activity. *Int J Biol Macromol*. 2024;264:130653. doi:10.1016/j.ijbiomac.2024.130653
33. Ghafouri-Fard S, Abak A, Tondro Anamag F, et al. 5-Fluorouracil: a narrative review on the role of regulatory mechanisms in driving resistance to this chemotherapeutic agent. *Front Oncol*. 2021;11:658636. doi:10.3389/fonc.2021.658636
34. Obireddy SR, Chintha M, Kashayi CR, Venkata KRKS, Subbarao SMC. Gelatin-coated dual cross-linked sodium alginate/magnetite nanoparticle microbeads for controlled release of doxorubicin. *ChemistrySelect*. 2020;5(33):10276–10284. doi:10.1002/slct.202002604
35. Obireddy SR, Lai W-F. Multi-component hydrogel beads incorporated with reduced graphene oxide for pH-responsive and controlled co-delivery of multiple agents. *Pharmaceutics*. 2021;13(3):313. doi:10.3390/pharmaceutics13030313
36. Costa P, Lobo JMS. Modeling and comparison of dissolution profiles. *Eur J Pharm Sci*. 2001;13(2):123–133. doi:10.1016/S0928-0987(01)00095-1
37. Singh P, Tyagi G, Mehrotra R, Bakhshi A. Thermal stability studies of 5-fluorouracil using diffuse reflectance infrared spectroscopy. *Drug Test Anal*. 2009;1(5):240–244. doi:10.1002/dta.41
38. Kannapiran N, Muthusamy A, Chitra P, Anand S, Jayaprakash R. Poly(o-phenylenediamine)/$NiCoFe_2O_4$ nanocomposites: synthesis, characterization, magnetic and dielectric properties. *J Magnet Magnet Mater*. 2017;423:208–216. doi:10.1016/j.jmmm.2016.09.095
39. Cheralayikkal S, Manoj K, Safna Hussan KP. Formulation and evaluation of a smart drug delivery system of 5-fluorouracil for pH-sensitive chemotherapy. *Heliyon*. 2022;8(7):e09926. doi:10.1016/j.heliyon.2022.e09926
40. Rao K, Reddy P, Rao K, Chang-Sik H. Chitosan-based interpenetrating polymeric network microgels for colon specific drug delivery of 5-Fluorouracil 2018. *Indian J Adv Chem Sci*. 2018;6(3):135–141.
41. Ramana EV, Naseem. Development, characterization and antibacterial properties of silver nanoparticles loaded sodium alginate/xanthan gum microbeads for drug delivery applications. *Int J Appl Pharm*. 2023;15(3):278–284. doi:10.22159/ijap.2023v15i3.47028
42. Lucena FRS, de Araújo LCC, Rodrigues M, et al. Induction of cancer cell death by apoptosis and slow release of 5-fluoracil from metal-organic frameworks Cu-BTC. *Biomed Pharmacother*. 2013;67(8):707–713. doi:10.1016/j.biopha.2013.06.003
43. Sabater I Serra R, Molina-Mateo J, Torregrosa-Cabanilles C, Andrio-Balado A, Duenas JMM, Serrano-Aroca Á. Bio-nanocomposite hydrogel based on zinc alginate/graphene oxide: morphology, structural conformation, thermal behavior/degradation, and dielectric properties. *Polymers*. 2020;12(3):702. doi:10.3390/polym12030702
44. Bhansali M, Dabholkar N, Swetha P, Dubey SK, Singhvi G. Solid oral controlled-release formulations. In: Azar AT, editor. *Modeling and Control of Drug Delivery Systems*. Academic Press; 2021:313–331.
45. Bahadoran M, Shamloo A, Nokoorani YD. Development of a polyvinyl alcohol/sodium alginate hydrogel-based scaffold incorporating bFGF-encapsulated microspheres for accelerated wound healing. *Sci Rep*. 2020;10(1):7342. doi:10.1038/s41598-020-64480-9
46. Zare-Akbari Z, Farhadnejad H, Furughi-Nia B, Abedin S, Yadollahi M, Khorsand-Ghayeni M. PH-sensitive bionanocomposite hydrogel beads based on carboxymethyl cellulose/ZnO nanoparticle as drug carrier. *Int J Biol Macromol*. 2016;93:1317–1327. doi:10.1016/j.ijbiomac.2016.09.110
47. Khalid I, Ahmad M, Minhas MU, Barkat K. Preparation and characterization of alginate-PVA-based semi-IPN: controlled release pH-responsive composites. *Polym Bull*. 2018;75(3):1075–1099. doi:10.1007/s00289-017-2079-y
48. Mirzaie Z, Reisi-Vanani A, Barati M. Polyvinyl alcohol-sodium alginate blend, composited with 3D-graphene oxide as a controlled release system for curcumin. *J Drug Deliv Sci Technol*. 2019;50:380–387. doi:10.1016/j.jddst.2019.02.005
49. Bohara RA, Thorat ND, Yadav HM, Pawar SH. One-step synthesis of uniform and biocompatible amine functionalized cobalt ferrite nanoparticles: a potential carrier for biomedical applications. *New J Chem*. 2014;38(7):2979–2986. doi:10.1039/c4nj00344f
50. Elbeltagi S, Alfassam HE, Saeedi AM, et al. A novel quercetin-loaded $NiFe_2O_4$@Liposomes hybrid biocompatible as a potential chemotherapy/hyperthermia agent and cytotoxic effects on breast cancer cells. *J Drug Deliv Sci Technol*. 2024;91:105203. doi:10.1016/j.jddst.2023.105203
51. Sukumar K, Bharathi M, Hirad AH, Alarfaj AA, Hussein-Al-Ali SH, Surya P. Development of chitosan-coated graphene oxide and iron oxide nanocomposites for targeted delivery of camptothecin to liver cancer cells. *Chem Biodivers*. 2025;22(2):e202401817. doi:10.1002/cbdv.202401817
52. Sundram S, Baskar S, Subramanian A. Green synthesized nickel doped cobalt ferrite nanoparticles exhibit antibacterial activity and induce reactive oxygen species mediated apoptosis in MCF-7 breast cancer cells through inhibition of PI3K/Akt/mTOR pathway. *Environ Toxicol*. 2022;37(12):2877–2888. doi:10.1002/tox.23644